Full Paper

Electrochemical Behavior of Nanoelectrode Ensembles in the Ionic Liquid [BMIm][BF_4]

Manuela De Leo,[a] *Ligia Maria Moretto*,[a] *Olivier Buriez*,[b] *Paolo Ugo*[a]*

[a] Department of Physical Chemistry, University Ca' Foscari of Venice, Santa Marta 2137, 30123 Venezia, Italy
[b] CNRS UMR 8640 "Pasteur", Ecole Normale Supérieure, Département de Chimie, 24, rue Lhomond, F-75231 Paris Cedex 05, France
*e-mail: ugo@unive.it

Received: July 26, 2008
Accepted: September 16, 2008

Abstract
The electrochemical behavior of nanoelectrode ensembles (NEEs), prepared by electroless plating of Au using microporous polycarbonate membranes as template, is tested in the ionic liquid [BMIm][BF_4]. The accessible potential window is significantly wider in [BMIm][BF_4] than in water, extending approximately, for 3.4 V vs. 1 V, respectively. The voltammetric behavior at NEEs of two redox probes, namely butyl viologen (BV^{2+}) and (ferrocenylmethyl) trimethylammonium (FA^+) are examined at different scan rates. In both cases, at scan rates higher than 200 mV/s sigmoidally shaped voltammograms typical of a pure radial diffusion regime are observed. At lower scan rates the voltammograms are peak shaped, as expected for total overlap diffusion conditions. This is the first time that the pure radial regime is obtained with NEEs made using commercially available polycarbonate templates, since in water solution only the total overlap regime is typically observed. This is explained as a consequence of the high viscosity of [BMIm][BF_4] which reflects in lowering of diffusion coefficients and smaller thickness of diffusion layers, for the same time scale, with respect to water solutions, but also the fact that the nanoelectrodes are slightly recessed helps in observing the pure radial regime. In order to make operative the pure radial condition it is indeed required that the thickness of diffusion layer at individual nanoelectrodes be smaller than the hemi-distance between neighboring nanoelectrodes. Examining the analytical performances achievable with NEEs in [BMIm][BF_4], it is shown that a limit is given by the decreased diffusion coefficients. Detection limits at NEEs in the ionic liquid are indeed higher than those obtained in water solutions. This notwithstanding, detections limits at NEEs in [BMIm][BF_4] are always improved with respect to those at conventional electrodes.

Keywords: Nanoelectrodes, Ensemble, Ionic liquid, Butyl viologen, Ferrocene derivatives, Diffusion

DOI: 10.1002/elan.200804414

1. Introduction

Nanoelectrode ensembles (NEEs) are nanotech based electroanalytical tools which find application in a variety of fields including trace electroanalysis and sensors [1, 2]. They are fabricated by growing metal nanowires in the pores of a template, typically a polycarbonate track-etched membrane. The density of the pores in the template determines the number of Au nanoelectrode elements per cm^2 of NEE surface and, correspondingly, the average distance between the nanoelectrode elements. NEEs can exhibit three distinct voltammetric response regimes depending on the thickness of the diffusion layer and distance between the nanoelectrode elements [3–5]: A) Total overlap (TO) Regime: when radial diffusion boundary layers overlap totally; B) Pure radial (PR): when the nanoelectrodes behave independently; C) Linear active: when the nanoelectrodes behave as isolated planar electrodes. The diffusion regime usually observed at NEEs fabricated from commercial track-etched membranes is the total overlap regime [1].

Under this diffusion regime, the faradaic current is directly proportional to all the geometric area of the ensemble (A_{geom}, that is area of the electrode elements plus area of the templating membrane), while the double-layer charging current (i_c) is proportional to the area of the electrode elements (active area, A_{act}). Thus detection limits at NEEs are 2–3 orders of magnitude lower than at regular electrodes [1–3, 6]. In the case of ensembles with the same active area, higher Faradaic currents are achieved indeed when operating under pure radial conditions [7]. The transition from the TO to the PR regime for NEEs has been demonstrated experimentally as a function of the template pore density [8], however the pure radial regime was achieved only with custom made membranes.

Notwithstanding these interesting analytical characteristics, NEEs application to a wider number of analytical problems suffers for some limits that are: a) narrow potential window accessible; b) accessibility, with commercial membranes, only at the total overlap diffusive regime.

The potential window accessible at gold disk NEEs (Au-NEEs) has been studied in detail in aqueous solutions [2],

where the cathodic limit is determined by the hydrogen evolution reaction and the anodic limit is given by the formation of gold oxide [1]. At the signal amplification levels required for micromolar (or lower) analyte concentrations, the potential window accessible at Au-NEEs extends between -0.300 V and $+0.800$ V vs. Ag/AgCl, at pH 7. Such limits can change with the nature of the metal of which the nanoelectrode is made, but no precise information is available up to now for materials different from gold. In principle, the accessible cathodic limit (related to hydrogen evolution) could be extended by using aprotic solvents. However, organic aprotic solvents cannot be used with NEEs since they dissolve the polycarbonate of the template.

Very recently, a large interest is rising on a new kind of electrolytes, named room temperature ionic liquids, or, more briefly, ionic liquids (ILs). ILs show interesting properties for electrochemical [9, 10], electroanalytical [11–14] and sensor [15] application. They are ionic aprotic solvents useful to dissolve water insoluble organics and metallorganics, to perform electrosynthesis and electroanalysis without the need of adding supporting electrolyte and avoiding parasitic reactions such as hydrogen evolution reaction which typically occurs in water solution at negative potential values. A characteristic of ILs which can play an important role in electrochemical application is the relatively high viscosity [9, 16]. In the majority of electrochemical application, a high viscosity of the electrolyte is undesired, since it means a slowing down of mass transport processes. However, in the case of NEEs, the increased viscosity can play a more complex and subtle role, since it can determine significant changes in the diffusive regime with respect to aqueous media.

Goal of the present research is to study the use of NEEs in [BMIm][BF_4], chosen as a well known and studied IL [17–19], with the purpose of examining peculiarities and possible advantages coming from the application of NEEs in ILs.

2. Experimental

2.1. Apparatus

Voltammetric measurements were performed with a CH660A apparatus controlled via PC, using IR-drop compensation. All electroanalytical measurements were carried out in a three-electrodes cell of small volume (5 mL). The working electrode was either a NEE or an Au-disk electrode, millimeter sized (diameter 3 mm), the counter electrode was a platinum coil and an Ag-wire was used as quasi-reference electrode. The half-wave potential ($E_{1/2}$) for the ferrocene/ferricinium couple, chosen as reference redox system, in this medium resulted equal to 0.320 V vs. Ag quasi-reference. All measurements were performed within a Faraday cage, at room temperature ($22 \pm 1\,^{\circ}C$), operating under a nitrogen atmosphere; the purging gas fluxed trough traps loaded with concentrated sulfuric acid, in order to prevent eventual entrance into the cell of humidity from the room environment.

2.2. Chemicals and Materials

Polycarbonate filtration membranes (SPI-Pore, 47 mm filter diameter, 6 μm filter thickness) with nominal pore diameter of 30 nm, pore density of 6×10^8 pores cm^{-2} and coated by the producer with polyvinylpyrrolidone were used as the templates to prepare the NEEs. The geometric area (area of the nanoelectrodes + area of the insulator among them) was 0.07 cm^2 while the active area (area of the nanoelectrodes alone) was 0.004 cm^2, average nanodisk diameter 30 nm. The NEE preparation procedure was described elsewhere [20–23]. Commercial gold electroless plating solution Oromerse Part B was purchased from Technic Inc. [BMIm][BF_4], purchased from Acros (minimal mole fraction purity 0.97), was dried with activated molecular sieves 4-A and kept 24 h at 40 °C in a vacuum oven before use [24]. (Ferrocenylmethyl)trimethylammonium hexafluorophosphate ($FA^+PF_6^-$) and butylviologen dibromide (BV^{2+}) were prepared as described in the literature [25, 26].

All other reagents were of analytical grade and used as received.

3. Results and Discussion

3.1. Accessible Potential Window

Figure 1A shows that the cathodic limit for NEEs in [BMIm][BF_4] extends to -2.0 V vs. Ag. In addition to the background current, two small signals are detected. The first, at approximately -0.750 V vs. Ag, is attributed to the reduction of trace oxygen, remaining even after careful deaeration of the sample. This signal increases indeed when the sample solution is oxygenated (aerated). The redox system at about -1.6 V is probably due to some impurity present in the IL. These trace signals are not detected at regular electrodes, in the same solution, so confirming the high sensitivity of NEEs for trace electroactive species. The anodic limit (Fig. 1B) is equal to 1.4 V vs. Ag, with an overall accessible potential window of approximately 3.4 V. This is much larger than the potential window of 1.1 V, accessible at NEEs in water solutions [2]. The potential window accessible with gold NEEs compares with the one accessible with flat gold electrodes (not shown). Note that the potential window accessible at gold electrodes (3.4 V) is slightly smaller than the one reported previously of about 4.2–4.6 V, observed when using glassy carbon or platinum as the electrode material [9]. As far as the application in [BMIm][BF_4] is concerned, it is worth to note that on the anodic side, the absence of OH^- ions prevents from the oxide formation, thus allowing a significant extension of the anodic limit of the accessible potential window. The fact that Au oxide formation is more difficult in the IL is also confirmed by the lack of observation of the typical oxide formation peaks also for regular gold disk electrodes (Au-disk) in [BMIm][BF_4] (not shown).

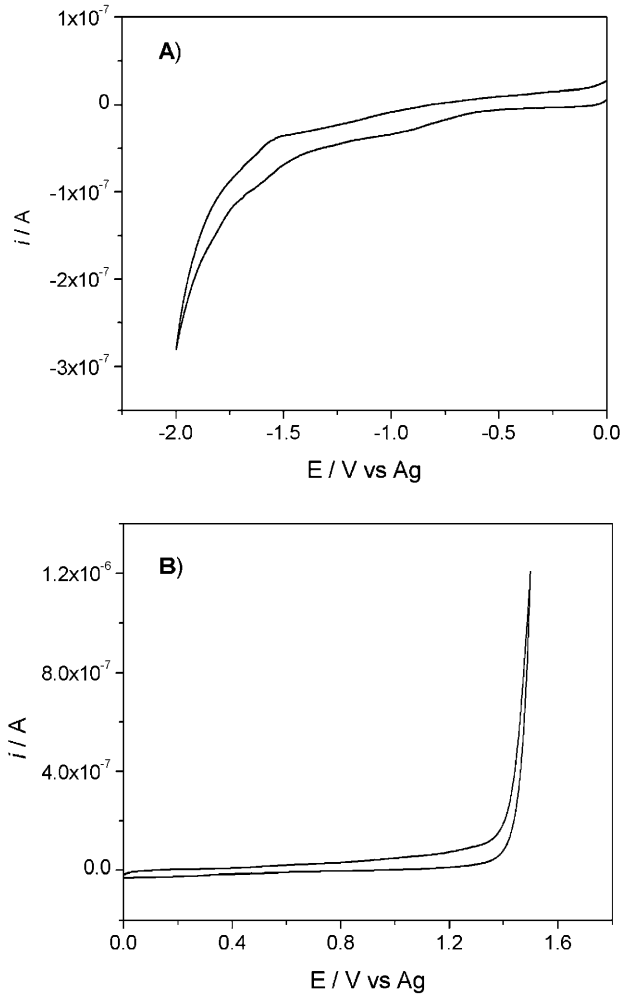

Fig. 1. Cyclic voltammograms recorded at NEE in [BMIm][BF_4]: A) cathodic scan; B) anodic scan. Scan rate 50 mV/s.

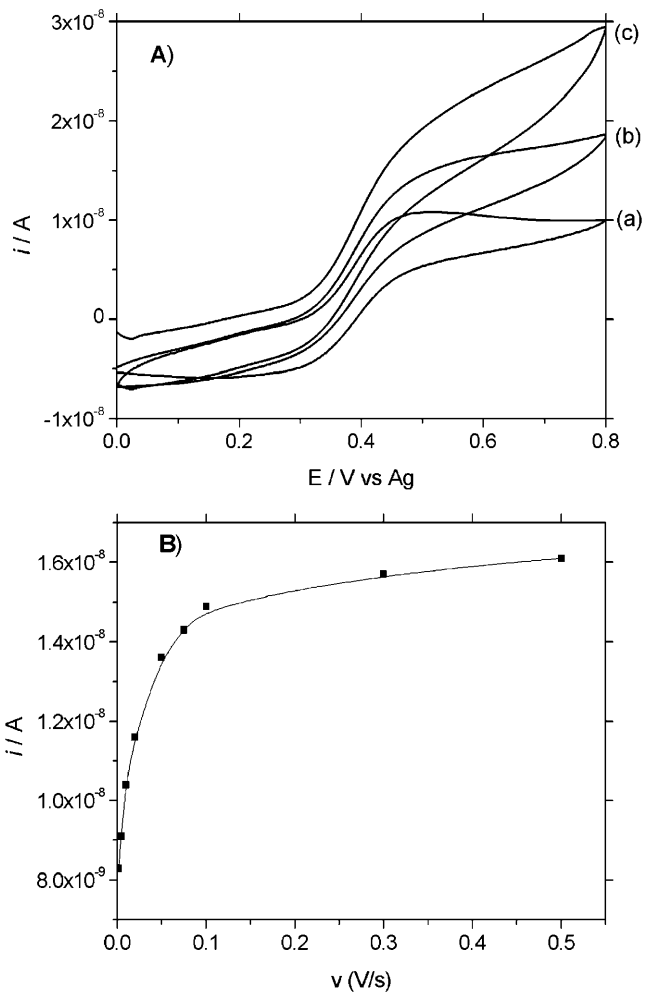

Fig. 2. A) Cyclic voltammograms recorded at NEE in 1×10^{-4} M FA^+, in [BMIm][BF_4] at different scan rates a) 2 mV/s, b) 20 mV/s, c) 100 mV/s. B) Scan rate dependence of the maximum current, that is plateau or peak current.

3.2. Voltammetry of FA^+

Figure 2A shows typical cyclic voltammograms recorded at different scan rates (2, 20, and 100 mV/s) at a NEE in 10^{-4} M FA^+ in [BMIm][BF_4]. At $v = 100$ mV/s, the CV pattern is sigmoidally shaped, although with a certain hysteresis between the forward and backward scans, with a maximum plateau current of about 1.8×10^{-8} A, while at quite low scan rate (2 mV/s) a peak is singled out.

The dependence of the maximum current (peak or plateau current) on the scan rate is plotted in Figure 2B. For scan rates < 50 mV/s, I_{max} depends strongly on v and results linear with the square root of the scan rate (not shown). When $v > 100$ mV/s, I_{max} tends to reach a constant value, independent of the scan rate. However, at high scan rates, the limiting as well as the background currents display a sloping trend, indicating a not-negligible ohmic component, probably caused by nonperfect sealing of the polycarbonate around the Au-nanofibers. The dependence of the maximum current on the scan rate indicates the occurrence of the TO regime at low scan rates which becomes PR at scan rates higher than 100 mV/s. Note that in aqueous solutions of the same analyte, in the same range of scan rates, NEEs always furnish peak shaped voltammograms with peak currents depending linearly on $v^{1/2}$, as expected when the total overlap regime is operative[1 – 3].

In order to investigate further the diffusion regime at NEEs in [BMIm][BF_4], the diffusion coefficient for FA^+ was determined, using a Au-disk electrode of calibrated electrode area.

As shown in Figure 3, a completely different situation respect to NEEs is observed using in the same solution the Au-disk electrode, since peak shaped CV are obtained, at any scan rate. ΔE_p values are always around 60 mV and a linear plot for I_p vs. $v^{1/2}$ is obtained (not shown). These evidence indicate the occurrence at the Au-disk electrode of a reversible, one-electron oxidation controlled by semi-infinite linear diffusion. Under linear diffusion conditions, from the slope of the I_p vs. $v^{1/2}$ plot, by applying the Randles – Sevcik equation it is possible to calculate D values. The D value so obtained is $(6 \pm 1) \times 10^{-8}$ cm^2/s. This

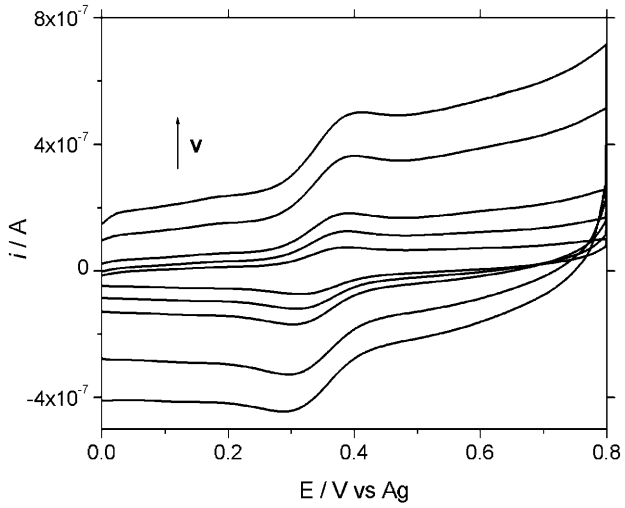

Fig. 3. Cyclic voltammograms recorded at Au-disk electrode in 1×10^{-3} M FA^+, in [BMIm][BF_4] at increasing scan rate (v): 20, 50, 100, 300, and 500 mV/s.

is almost two orders of magnitude lower than the value recorded for the same analyte in water solution, namely 4×10^{-6} cm^2/s [27] or for ferrocene and its derivatives in acetonitrile solutions, where D values were of the order of 10^{-5} cm^2 s^{-1} [28]. This trend agrees with the high viscosity of [BMIm][BF_4] which is higher than 100 cP, (reported as 112 cP [29], 154 cP [16] or 180 cP [9], depending on the source). On the basis of the Stokes – Einstein equation [9], the diffusion coefficient is inversely proportional to the viscosity. Similarly small diffusion coefficient values were measured in [BMIm][BF_4] for other electroactive molecules such as Ni (salen) ($D = 1.8 \times 10^{-8}$ cm^2/s [24]), iodine ($D = 2 \times 10^{-7}$ cm^2/s [30]), ferrocene and ferricinium ($D = 1.8 \times 10^{-7}$ cm^2/s and 1.3×10^{-7} cm^2/s, respectively [31]).

In the case of NEEs, at a fixed scan rate (i.e. fixed experimental time window), lowering of diffusion coefficients means decrease the radius of diffusion hemisphere around each nanoelectrode. When diffusion hemispheres are lower then the hemidistance between the electrodes, pure radial diffusion conditions prevail. This means that the transition from total overlap to radial control is observed at lower scan rates in media where diffusion coefficients are smaller, that is, the viscosity is higher. This is the case of [BMIm][BF_4], where such transition occurs at scan rates between 50 – 100 mV/s, in comparison with water where the total overlap regime is the prevailing regime over a very wide range of scan rates, e.g. from 10 mV/s to 10 V/s.

Using the theoretical model applied to disk-ultramicroelectrodes operating under pure radial conditions, steady state current can be calculated by Equation 1:

$$I_{ss}^{NEE} = 4\ nFDCr\ A_{geom}\ d \quad (1)$$

where n is the number of electron exchanged, F is the Faraday constant, D is the diffusion coefficient, C is the concentration, r is the radius of the nanoelectrodes, A_{geom} is the overall geometric area of the ensemble (nanodisk + polycarbonate exposed to the sample solution) and d is the nanoelectrodes density; note that the product $A_{geom}\ d$ gives the total number of nanoelectrodes in contact with the sample solution.

By substitution of proper parameters in Equation 1, the value expected for an ensemble of inlaid nanodisks is $I_{ss}^{NEE} = 1 \times 10^{-7}$ A. Such a theoretical current is 5 – 6 times larger than the experimental value, above reported. A possible explanation of this discrepancy is that the nanoelectrodes are partially recessed so that Equation 2 [32] should be used instead of Equation 1.

$$I_{lim} = 4\pi\ nFCDr^2/(4\ L + \pi r) \quad (2)$$

where L = recessed depth.

From the value of experimental plateau currents and Equations 1 and 2, the recession depth can be evaluated in the order of 30 – 50 nm. This recession can be possibly originated during the cleaning of the outer surface of the NEE during the preparation of the ensemble [22].

It is interesting to stress that, when NEEs operate in TO regime, the peak current is always proportional to A_{geom} so that such a small recession of the nanoelectrodes has no effect on the voltammetric patterns.

Another element supporting the possibility of a small recession of the nanoelectrodes is the fact that in [BMIm][BF_4], for inlaid nanoelectrodes with average distance between them of 200 nm [1], the transition between TO and PR regime should be observed at scan rates higher than 100 – 200 mV/s.

With electrodes as small as those used here, by electron microscopy analyses it is almost impossible to know whether one of these situations really occur, particularly in the case when defects in the NEE are not too heavy. Moreover, the electrochemical characterization in water is not very informative unless these defects are very heavy [33]. In fact, in water, as long as the total overlap conditions hold, voltammograms of an ensemble of perfect nanodisks do not differ, except for the capacitive current, from the one of an ensemble where some of the electrodes are slightly recessed or slightly protruding [21].

3.3. Butyl Viologen

Figure 4 shows the cyclic voltammograms recorded at different scan rates at a NEE in 5×10^{-3} M BV^{2+}, [BMIm][BF_4] solution. Two following reduction processes are observed with reduction peak potentials at about -0.300 V and -0.720 V vs. Ag, respectively. Comparison with the literature referring to the electrochemical reduction of BV^{2+} in acetonitrile solutions [34, 35] indicate that the two processes correspond to the following reactions:

$$BV^{2+} + e^- \rightleftharpoons BV^+ \quad (3)$$

$$BV^+ + e^- \rightleftharpoons BV^\circ \quad (4)$$

The CVs recorded at scan rate lower than 100 mV/s (Fig. 4A) are peak shaped with a Cottrellian decrease in the current between the first and the second reduction process. At higher scan rates (Fig. 4B) the current between the two peaks does not decrease and the CVs tend to a partially sigmoidal shape. This trend is stressed by comparing the CVs obtained with the NEE with those recorded in the same solution with an Au-disk electrode (see Fig. 5), where peak shaped voltammograms are recorded at all of the scan rates explored with peak currents increasing linearly with $v^{1/2}$ (not shown). Interestingly, at the NEEs, the maximum current for the second reduction process is slightly larger than the current for the first reduction. This effect is more evident at high scan rates, that is under pure radial control, and smaller at low scan rate, under total overlap conditions. Note that current signals under pure radial conditions depend directly on D, while under total overlap, they depend on $D^{1/2}$. This evidence suggests that the possible cause behind this difference in voltammetric current for the two processes be the fact that the diffusion coefficient for BV^{2+} is slightly smaller than that for BV^{+}.

For NEEs, the results of the analysis of the current for the first reduction process as a function of the scan rate are reported in Figure 4C. For $v < 200$ mV/s, the current increases steeply with v, depending linearly on $v^{1/2}$ up to $v <$ 200mV/s. For $v > 400$ mV/s, a flattening of this dependence is observed, with currents tending to reach a plateau at about 3×10^{-6} A. Similarly with the FA^{+} case, the characteristics of the CVs recorded at scan rates lower than 100 mV/s indicate that the total overlap regime is operative, while, at higher scan rates the process tends to be under radial control.

At constant scan rate, both at NEEs and Au-macro, reduction currents for both processes increase linearly with the BV^{2+} concentration (not shown) up to, at least, 10^{-2} M BV^{2+}.

On the other hand, the analysis of the scan rate dependence for the Au-disk electrode indicates planar diffusion at all the scan rates explored. From the slope of the linear I_p vs. $v^{1/2}$ plot, by applying the Randles–Sevcik equation, a diffusion coefficient of 3.5×10^{-8} cm^2/s is obtained for BV^{2+} in [BMIm][BF_4]. Again, this is a quite small diffusion coefficient value in agreement with the high viscosity of [BMIm][BF_4] and in the same range as diffusion coefficients for other analytes, in the same IL.

The electrochemical reduction of other viologens, namely methyl viologen, was previously studied at NEEs in water solution [2]; this could not be done for BV^{2+} since this more hydrophobic viologen does not dissolve in water. Note, however, that for the methyl viologen case in water the study had to be limited to the first reduction process since the second one takes place beyond the cathodic limit accessible at Au-NEEs in water. On the contrary, the use of [BMIm][BF_4] allowed us to achieve a multiple goal that is to extend the study to the second reduction process of a water insoluble viologen using NEEs.

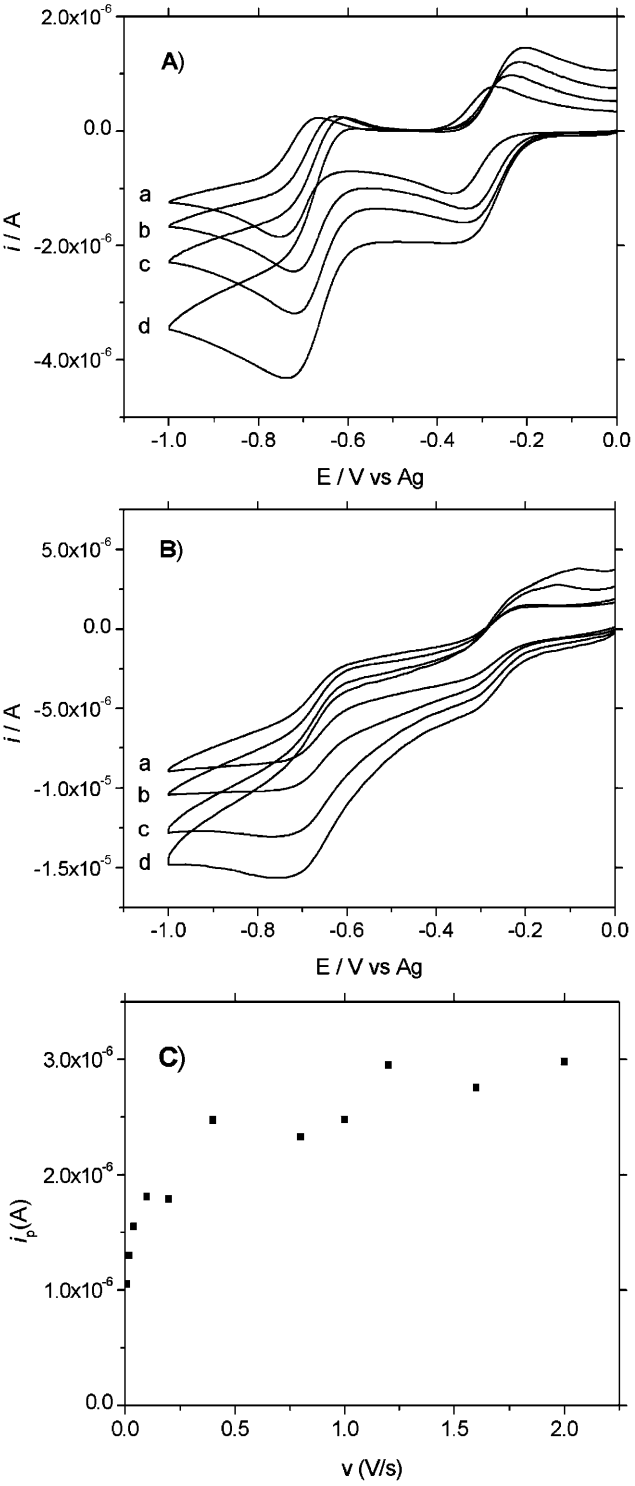

Fig. 4. Cyclic voltammograms recorded at a NEE in 5×10^{-3} M BV^{2+}, in [BMIm][BF_4] at different scan rates: A) a) 10, b) 20, c) 40, and d) 100 mV/s; B) a) 200, b) 400, c) 1200, and d) 2000 mV/s. C. Current of the first cathodic peak as a function of the scan rate.

3.4. Detection Limits in [BMIm][BF_4]

In order to examine the role of the change in viscosity and diffusion regime on the analytical performances of NEEs,

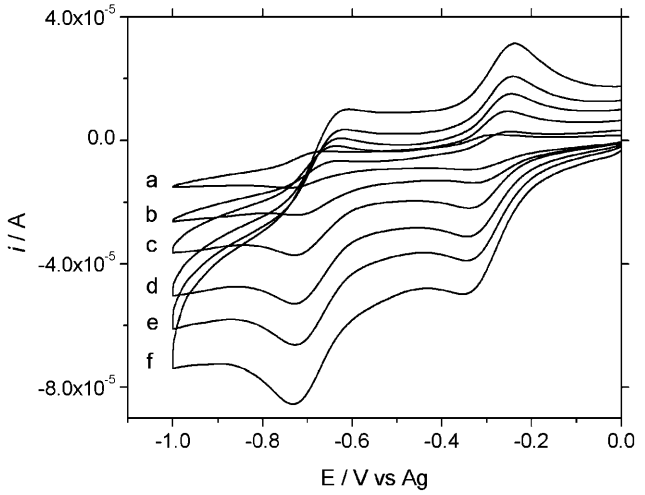

Fig. 5. Cyclic voltammograms recorded at Au-disk electrode in 5×10^{-3} M BV^{2+} , in [BMIM][BF_4] at increasing scan rate: a) 40, b) 100, c) 400, d) 800, e)1200, and f) 1600 mV/s (higher scan rates = higher peak currents).

detection limits at NEEs and at the Au-macro in [BMIm][BF_4] were evaluated and compared. Because of the availability of a similar comparison in water solution for the FA^+ analyte, we based this part of the study on this molecule.

Figure 6A shows the CV recorded at a NEE after addition of increasing concentration of FA^+ and Figure 6B reports the relevant linear calibration plot. The same was done with the Au-disk electrode and relevant CVs are shown in Figure 7.

The background noise was obtained as the standard deviation, σ_b, of repeated measurements ($n = 10$) of the blank current in correspondence of the FA^+ peak potential. Detection limits were calculated as:

$$DL = 3\sigma_b/m \quad (5)$$

where m is the sensitivity that is the slope of the linear calibration plot. DL for FA^+ in [BMIm][BF_4] was 5×10^{-6} M at the NEE and 18×10^{-6} M at the Au-disk. DL values obtained for the same analyte in water solution [6] were 0.05×10^{-6} M and 20×10^{-6} M for the NEE and Au-disk, respectively.

Both in water and [BMIm][BF_4], DLs are improved with the NEE, however this improvement is lower in the *IL*. This agrees on one hand with the lowering of the sensitivity caused by the decrease in diffusion coefficient values typical of [BMIm][BF_4], on the other by the fact that under radial control, less than 100% of the overall geometric area of the NEE contributes to the signal. Note that for our comparison the overall geometric area both of the NEE and Au-macro were kept constant.

As far as BV^{2+} is concerned, DL at the NEE in [BMIm][BF_4] was 1.1×10^{-5} M, when the calibration plot is performed on the first reduction peak. Increased DL

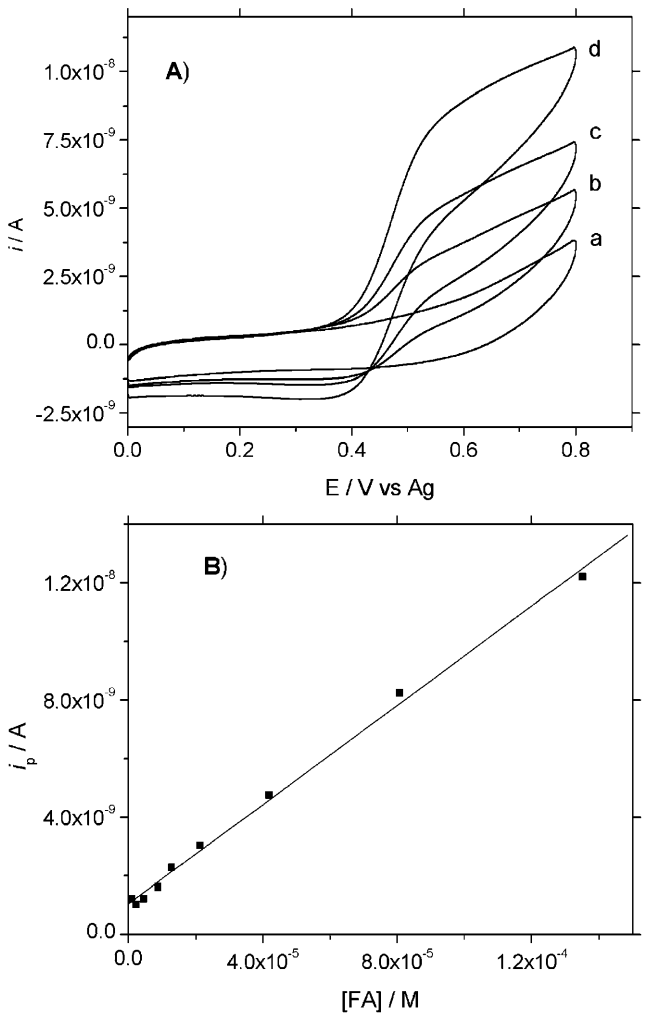

Fig. 6. A) Cyclic voltammograms recorded at NEE in FA^+ [BMIm][BF_4] solution at different concentrations: a) 4×10^{-6} M, b) 2×10^{-5} M, c) 4×10^{-5} M, d) 8×10^{-5} M, scan rate 20 mV/s. B) Relevant calibration plot.

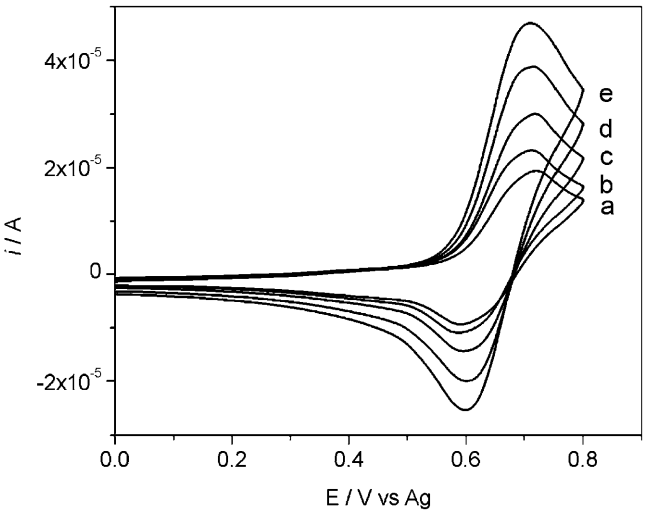

Fig. 7. Cyclic voltammograms recorded at Au-disk electrode in [BMIm][BF_4] solution at increasing FA^+ concentrations: a) 6×10^{-3} M, b) 8×10^{-3} M, c) 9×10^{-3} M, d) 12×10^{-3} M, e) 13×10^{-3} M), scan rate 50 mV/s.

agrees with lower diffusion coefficient for BV^{2+} with respect to FA^{+}.

4. Conclusions

The use of NEEs in [BMIm][BF_4] showed some interesting peculiarities with respect to the behavior observed in aqueous solutions. As expected, the accessible potential window is significantly extended so allowing the detection of analytes which are electroactive also at rather negative or positive potential values. At variance with organic solvent, which can dissolve the polycarbonate in which the NEEs are made, the IL does not damage the templating membrane. A relevant role is played by the high viscosity of the ionic liquid which causes a decrease in diffusion coefficients and, therefore, a lower analytical sensitivity with respect to aqueous solutions. This is a feature common both for NEEs and for regular electrodes. What is peculiar for NEEs in IL is that the thinning of diffusion layer allows one to obtain voltammetric signals both under pure radial regime and total overlap regime, depending on the scan rate. This contrasts with the situation typically encountered with NEEs in water solution where the total overlap regime is always dominating. Interestingly, the accessibility to the pure radial regime put in evidence some morphological peculiarities in the NEEs which cannot be observed in water. Comparison between theoretical and experimental currents under pure radial conditions indicated, in fact, a slight degree of recession of the nanoelectrodes with respect to the surface of the templating membrane.

From an analytical viewpoint it is worth stressing that NEEs gave detection limits improved with respect to regular electrodes also in IL, however this advantage is not as dramatic as in water solutions. The use of NEEs for analysis in ILs is therefore recommended only when strictly necessary, that is for those analytes too hydrophobic to be soluble in water and/or detectable only at potential values outside the potential window accessible with NEEs in water.

5. Acknowledgements

Financial support by MIUR (Rome, Cofin 2006) is grateful acknowledged. We thank Enrico Ferraro and Chiara Vallese for performing some preliminary experiments.

6. References

[1] V. P. Menon, C. R. Martin, *Anal. Chem*. **1995**, *67*, 1920.
[2] B. Brunetti, P. Ugo, L. M. Moretto, C. R. Martin, *J. Electroanal. Chem*. **2000**, *491*, 166.
[3] P. Ugo, L. M. Moretto, F. Vezzà, *ChemPhysChem* **2002**, *3*, 917.
[4] C. Amatore, in *Physical Electrochemistry* (Ed: I. Rubinstein), Marcel Dekker, New York, **1995**, p. 131.
[5] C. La Fratta, D. R. Walt, *Chem.Rev.* **2008**, *108*, 614.
[6] P. Ugo, L. M. Moretto, S. Bellomi, V. P. Menon, C. R. Martin, *Anal. Chem*. **1996**, *68*, 4160.
[7] H. J. Lee, C. Beriet, R. Ferrigno, H. H. Girault, *J. Electroanal. Chem*. **2001**, *502*, 138.
[8] J. C. Hulteen, V. P. Menon, C. R. Martin, *J. Chem. Soc. Faraday Trans.* **1996**, *92*, 4029.
[9] M. Galinski, A. Lewandowski, I. Stepniak, *Electrochim. Acta* **2006**, *51*, 5567.
[10] T. Tsuda, C. L. Hussey, *The Electrochemical Society – Interface* – Spring **2007**, p. 42.
[11] M. C. Buzzeo, R. G. Evans, R. G. Compton, *ChemPhysChem* **2004**, *5*, 1106.
[12] J. Liu, J. A. Jönsson, G. Jiang, *Trends Anal. Chem.* **2005**, *24*, 20.
[13] X. Ji, C. E. Banks, D. S. Sivester, L. Aldous, C. Hardacre, R. G. Compton, *Electroanalysis* **2007**, *19*, 2194.
[14] C. A. Brooks, A. P. Doherty, *Electrochem. Commun.* **2004**, *6*, 867.
[15] M. C. Buzzeo, C. Hardacre, R. G. Compton, *Anal. Chem.* **2004**, *76*, 4583.
[16] P. Hapiot, C. Lagrost, *Chem Rev.* **2008**, *108*, 2238.
[17] P. A. Z. Suarez, V. M. Selbach, J. E. L. Dullius, S. Einsloft, C. M. S. Piatinicki, D. S. Azambuja, R. F. de Souza, J. Dupont, *Electrochim. Acta* **1997**, *42*, 2533.
[18] M. G. Freire, P. J. Carvalho, A. M. Fernandes, I. M. Marrucho, A. J. Queimada, J. A. P. Coutinho, *J. Colloid Interf. Sci.* **2007**, *314*, 621.
[19] J. Vila, L. M. Varela, O. Cabeza, *Electrochim. Acta* **2007**, *52*, 7413.
[20] P. Ugo, N. Pepe, L. M. Moretto, M. Battagliarin, *J. Electroanal. Chem*. **2003**, *560*, 51.
[21] M. De Leo, A. Kuhn, P. Ugo, *Electroanalysis* **2007**, *19*, 227.
[22] P. Ugo, L. M. Moretto, in *Handbook of Electrochemistry* (Ed: C. G. Zosky), Elsevier, Amsterdam, **2007**, ch. 16, sect. 16.2, pp. 678 – 709.
[23] M. De Leo, F. C. Pereira, L. M. Moretto, P.Scopece, S. Polizzi, P. Ugo, *Chem. Mater*. **2007**, *19*, 5955.
[24] B. K. Sweeney, D. G. Peters, *Electrochem. Commun*. **2001**, *3*, 712.
[25] A. Lombardo, T. I. Bieber, *J. Chem. Education* **1983**, *60*, 1080.
[26] J. Hanzlik, Z. Samec, *Collect. Czech, Chem. Commun*. **1987**, *52*, 830.
[27] E. Sabatani, I. Rubinstein, *J. Phys. Chem*. **1987**, *91*, 6663.
[28] J. E. Baur in *Handbook of Electrochemistry* (Ed: C. G. Zosky), Elsevier, Amsterdam, **2007**, ch. 19, p. 845.
[29] P. Bonhote, A. P. Dias, N. Papageorgiou, K. Kalyanasundaram, M. Gratzel, *Inorg. Chem*. **2006**, *35,* 1168.
[30] Y. Zhang, J. B. Zheng, *Electrochim. Acta* **2007**, *52*, 4082.
[31] E. I. Rogers, D. S. Silvester, D. L. Poole, L. Aldous, C. Hardacre, R. G. Compton, *J. Phys. Chem. C* **2008**, *112*, 2729.
[32] D. W. M. Arrigan, *Analyst* **2004**, *129*, 1157.
[33] F. C. Pereira, L. M. Moretto, M. De Leo, M. V. Boldrin Zanoni, P. Ugo, *Anal. Chim. Acta* **2006**, *575*, 16.
[34] B. Brunetti, P. Ugo, *J. Electroanal. Chem*. **1999**, *460*, 38.
[35] L. Bird, A. T. Kuhn, *Chem. Soc. Rev.* **1981**, *10*, 49.

